Missouri University of Science and Technology
Scholars' Mine

Electrical and Computer Engineering Faculty Research & Creative Works

Electrical and Computer Engineering

01 Jun 2022

Distributed Fiber Optic Sensing with Enhanced Sensitivity based on Microwave-Photonic Vernier Effect

Chen Zhu
Misssouri University of Science and Technology, cznwq@mst.edu

Muhammad Roman

Yiyang Zhuang

Jie Huang
Missouri University of Science and Technology, jieh@mst.edu

Follow this and additional works at: https://scholarsmine.mst.edu/ele_comeng_facwork

 Part of the Electrical and Computer Engineering Commons

Recommended Citation

C. Zhu et al., "Distributed Fiber Optic Sensing with Enhanced Sensitivity based on Microwave-Photonic Vernier Effect," *Optics Letters*, vol. 47, no. 11, pp. 2810 - 2813, Optica, Jun 2022.
The definitive version is available at https://doi.org/10.1364/OL.461307

This Article - Journal is brought to you for free and open access by Scholars' Mine. It has been accepted for inclusion in Electrical and Computer Engineering Faculty Research & Creative Works by an authorized administrator of Scholars' Mine. This work is protected by U. S. Copyright Law. Unauthorized use including reproduction for redistribution requires the permission of the copyright holder. For more information, please contact scholarsmine@mst.edu.

Optics Letters

Distributed fiber optic sensing with enhanced sensitivity based on microwave-photonic Vernier effect

Chen Zhu,[1,3] Muhammad Roman,[2] Yiyang Zhuang,[1] and Jie Huang[2,4]

[1]Research Center for Optical Fiber Sensing, Zhejiang Laboratory, Hangzhou 311100, China
[2]Department of Electrical and Computer Engineering, Missouri University of Science and Technology, Rolla, Missouri 65409, USA
[3]e-mail: chenzhu@zhejianglab.com
[4]e-mail: jieh@mst.edu

Received 19 April 2022; accepted 8 May 2022; posted 10 May 2022; published 25 May 2022

The Vernier effect has been widely used in the field of measurement and instrumentation for sensitivity enhancement. Single-point optical fiber sensors based on the Vernier effect have been extensively reported in recent years. In this Letter, for the first time, a distributed optical fiber sensor based on microwave photonics with improved sensitivity enabled by the Vernier effect is demonstrated. Distributed sensing is realized by interrogating a Fabry–Perot interferometer (FPI) array formed by cascaded reflectors along an optical fiber using an optical carrier-based microwave interferometry (OCMI) system. A reference FPI is also included in the system. The interferogram of each of the sensing FPIs can be unambiguously reconstructed and superimposed with the reconstructed interferogram of the reference FPI to generate the Vernier effect. By tracking the spectral shift of the envelope signals in the superimposed spectra, the measurement sensitivities of the sensing FPIs can be significantly improved. A simple direct modulation-based OCMI system is used in the proof-of-concept demonstration, showing sensitivity-enhanced distributed sensing capability. Moreover, the sensitivity amplification factor can be adjusted by varying the optical length difference of the sensing and reference FPIs, similar to that of Vernier effect-based single-point optical fiber sensors. © 2022 Optica Publishing Group

https://doi.org/10.1364/OL.461307

The Vernier effect is a fundamental technique that is used to realize high-precision and high-accuracy length measurements based on Vernier calipers. In recent years, the so-called optical Vernier effect has been proposed, which is generated by superimposing responses of a sensing interferometer and a reference interferometer with slightly different optical path differences (OPDs) [1]. Instead of monitoring the spectral shift of the sensing interferometer, as is often the case for traditional interferometric sensors, the shift of the envelope signal in the superimposed spectrum of a Vernier-effect-based sensor is tracked. Importantly, the shift of the envelope is significantly improved thanks to the Vernier effect; a closer OPD between the reference and sensing interferometers results in a larger amplification factor. Taking advantage of sensitivity amplification enabled by the Vernier effect, various high-sensitivity optical fiber sensors have been demonstrated based on different configurations, such as the Fabry–Perot interferometer (FPI) [2–5], the Mach–Zehnder interferometer [6,7], and the Sagnac interferometer [8,9]. These sensitivity-enhanced sensors were demonstrated for measuring a diverse array of physical and chemical quantities [1,10]. In addition to the optical domain, the microwave-photonic Vernier effect was recently reported and used to improve the measurement sensitivity of microwave-photonic sensors [11–13]. However, to the best of our knowledge, the application of the Vernier effect for sensitivity enhancement is only limited to single-point optical fiber sensors. In this Letter, for the first time, a method is proposed and demonstrated showing that the Vernier effect can be used in a distributed optical fiber sensor, leading to the development of a high-sensitivity spatially distributed sensing system.

FPIs are one of the most widely used sensing configurations due to the ease of fabrication, compactness, and the possibility of multiplexing [14]. Multiple in-fiber reflectors were fabricated along an optical fiber to form an in-fiber FPI array for fully distributed sensing [15–17]. Different techniques have been demonstrated to interrogate the FPI array, including optical frequency domain reflectometry (OFDR) and optical carrier-based microwave interferometry (OCMI). The OCMI is a microwave-photonic measurement technique, where a microwave-modulated optical signal is launched into the fiber under test for probing distributed changes along the fiber [17]. Integrating advantages of two different arenas, i.e., microwave and optics, the OCMI technique brought in some features that are especially attractive when it comes to sensing applications, such as low dependence on multimode interference and insensitivity to variations of the polarization state of the probing light [17–21]. In this article, by combining the OCMI interrogation technique and an FPI array, the first implementation of the Vernier effect in a distributed optical fiber sensor for sensitivity improvement is demonstrated.

A schematic of the proposed system is shown in Fig. 1(a). The intensity-modulated optical signal is sent into an optical fiber coupler. The two pigtail fibers from the coupler are considered as the sensing arm and reference arm. In the reference arm, two partial reflectors are fabricated (i.e., R_1 and R_2) to form

an FPI, which is considered as the reference FPI. The sensing arm includes multiple reflectors that are cascaded along the optical fiber line (i.e., S_1, S_2, ...), and any two adjacent reflectors form a sensing FPI (e.g., reflector S_i and S_{i+1} form the ith sensing FPI), whose reflection spectrum is a function of the length and the refractive index of the optical fiber in-between the two reflectors. Therefore, an FPI array is constructed in the sensing arm, and each of the FPIs can be used for localized sensing. Importantly, the OPD of the FPIs should be sufficiently larger than the coherence length of the light source so that the system can operate at an incoherent regime. The reflected optical signal is routed to a photodetector and then sent to the microwave detector. Sweeping the frequency (Ω) of the microwave modulation signal and using synchronized detection, the normalized superimposed complex spectrum of the reference arm and sensing arm of the system can be obtained and can be expressed as

$$S_{21}(\Omega) = \sum_{p=1}^{N} M\Gamma_p{}^2 A^2 e^{-j\Omega\frac{2n_p z_p}{c}}, \tag{1}$$

where M is the modulation depth of the intensity-modulated light; A is the amplitude of the probing light; Γ_p represents the reflection coefficient of the pth reflector; N denotes the total number of reflectors in the system; n_p and z_p are the refractive index and length of the fiber line of the pth reflector, respectively; and c is the speed of light in vacuum. By applying an inverse Fourier transform (IFT) to the complex S_{21} signal, the time-domain signal of the system can be obtained by

$$X(t) = \sum_{p=1}^{N} M\Gamma_p{}^2 A^2 \delta\left(t - \frac{2n_p z_p}{c}\right), \tag{2}$$

where t is the time variable. According to Eq. (2), the time-domain signal includes a series of pulses with different time delays, which are determined by the spatial locations of the reflectors. The amplitude of each of the pulses is predicated by the reflection coefficient of the reflector. The obtained time-domain signal can be subsequently transformed into the spatial domain signal, as illustrated in Fig. 1(b), from which the spatial location of each reflector can be easily recognized. Applying a gate function to any two adjacent reflectors and followed by a Fourier transform (FT), the microwave interferogram for the specific FPI (i.e., the magnitude spectrum) can be reconstructed:

$$Mag = S_{21}(\Omega) * [G(\Omega)\exp(-j\Omega\tau_0)], \tag{3}$$

where $G(\Omega)$ and τ_0 are the FT result and time delay of the gate function, respectively. A time gate is first applied to select the two reference reflectors to reconstruct the interferogram of the reference FPI. Another time gate is applied to the sensing reflectors (e.g., S_i and S_{i+1}) so that the interferogram of the ith sensing FPI is reconstructed. By sliding the gate function to cover all the sensing reflectors and correspondingly choosing appropriate parameters of the gate function, interferograms of all the sensing FPIs can be obtained. Traditionally, by tracking the spectral shift of each of the FPI interferograms and integrating the localized information, dark-zone free distributed sensing can be achieved [17]. At this point, the Vernier effect is introduced to amplify the measurement sensitivity of each of the sensing FPIs and thereby improve the overall sensitivity for distributed sensing. Let us take the ith sensing interferometer as an example. Instead of directly monitoring the spectral shift of its interferogram, the interferograms of the reference FPI and the ith sensing FPI are

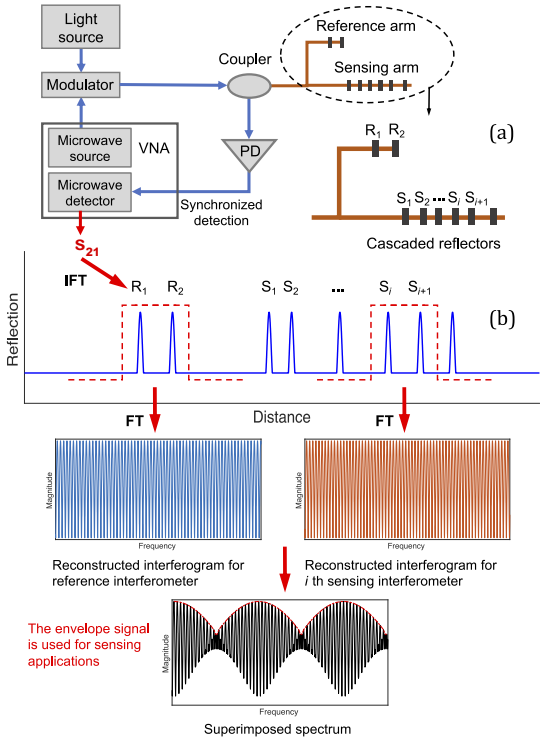

Fig. 1. Vernier-effect-amplified distributed optical fiber sensing system based on OCMI. (a) Schematic of the system. VNA, vector network analyzer; PD, photodetector. (b) Illustration of the signal processing procedures of the system for sensitivity-enhanced sensing. The envelope in the superimposed spectrum (indicated by the red curve) is used for sensing applications with enhanced sensitivity. FT, Fourier transform; IFT, inverse Fourier transform.

superimposed to obtain a typical amplitude-modulated signal, as shown in Fig. 1(b), to generate the Vernier effect. The free spectral range (FSR) of the envelope signal can be predicted by

$$FSR_{en} = \frac{FSR_{ref} FSR_{sen}}{|FSR_{ref} - FSR_{sen}|}, \tag{4}$$

where FSR_{ref} and FSR_{sen} represent the FSR of the reference and sensing interferometers, respectively. Then, the shift of the envelope in the superimposed spectrum is tracked for sensing applications. Importantly, when the sensing FPI is subject to an external perturbation, the shift of the envelope is magnified compared with that of the original interferogram of the sensing FPI, thanks to the Vernier effect. Moreover, the closer the OPD between the sensing and reference interferometers, the larger the amplification factor will be expected based on

$$V = \frac{OPD_{sen}}{OPD_{sen} - OPD_{ref}}, \tag{5}$$

where OPD_{sen} and OPD_{ref} represent the OPD of the sensing and reference interferometers, respectively. Different from the traditional Vernier-effect-based optical fiber sensors where the system performance (e.g., the largest amplification factor) is limited by the bandwidth of the light source, the proposed system is limited by the frequency bandwidth of the microwave modulation signal [13]. The bandwidth of the light source in the system does not affect the largest amplification factor that can be achieved, but it does affect the overall system performance, as

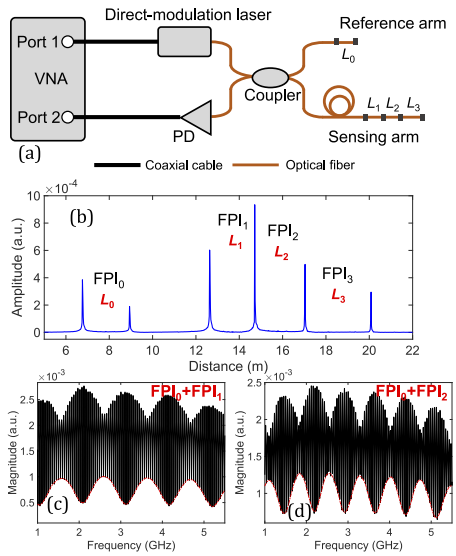

Fig. 2. Proof-of-concept demonstration. (a) Schematic of the direct-modulation OCMI system. (b) Spatial domain signal of the system. Superimposed spectrum for (c) $FPI_0 + FPI_1$ and (d) $FPI_0 + FPI_2$. The red curves indicate the envelopes that would be used for sensing applications in later experiments.

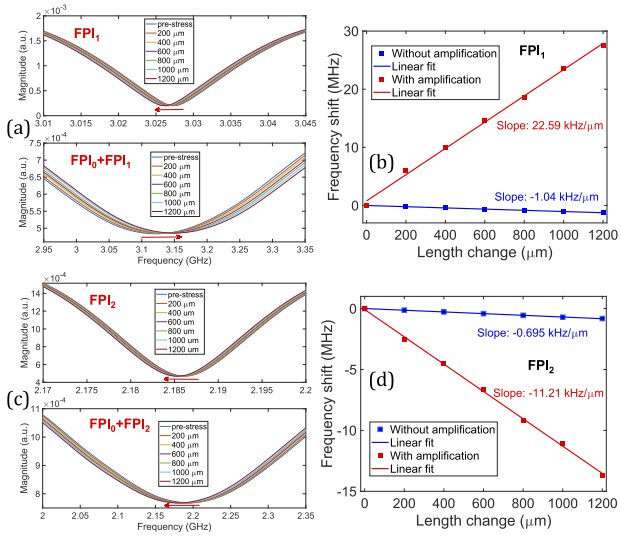

Fig. 3. Sensitivity-enhanced distributed sensing. (a) Reconstructed interferograms of FPI_1 and curve-fitted envelope signals of the superimposed spectra of $FPI_0 + FPI_1$ centered at ~3 GHz for different settings of length change. (b) Shift in dip frequency of the interferograms and the envelope signals shown in panel (a) as a function of length change. (c) Reconstructed interferograms of FPI_2 and envelope signals of the superimposed spectra of $FPI_0 + FPI_2$ centered at ~2 GHz for different settings of length change. (d) Shift in dip frequency of the interferograms and the envelope signals shown in panel (c) as a function of length change.

demonstrated in Ref. [22]. Note that in addition to the envelope highlighted in Fig. 1(b), the bottom envelope can also be used for sensing, as shown in later experiments.

A simple direct-modulation OCMI system was constructed for the proof-of-concept demonstration, as shown in Fig. 2(a). Details about the OCMI system can be found in recent work [23]. A total of six reflectors were included in the system, which were simply created by introducing small air gaps between the lead-in and lead-out optical fibers. The first two reflectors were used to form a reference FPI (i.e., FPI_0) with a physical length of L_0, and the four reflectors in the sensing arm formed three cascaded sensing FPIs (i.e., FPI_1, FPI_2, and FPI_3) with lengths of L_1, L_2, and L_3. Figure 2(b) shows the measured spatial domain signal of the system, where six pulses can be observed, corresponding to the six reflectors. The peak amplitudes are different due to the fact that the air-gap-based reflectors are not identical in terms of the gap distance [23], which will not affect the system performance. The lengths of the FPIs were determined to be: $L_0 = 2.174$ m, $L_1 = 2.081$ m, $L_2 = 2.322$ m, and $L_3 = 3.047$ m. Note that ideally, the physical lengths of the sensing FPIs should be the same so that for a given reference FPI, the sensitivity amplification factor for all sensing FPIs is the same. Here, the length of the sensing FPIs is set to be different to demonstrate that the amplification factor is a function of the OPD difference between the sensing FPI and the reference FPI, that is, to verify Eq. (5). Following the procedures illustrated in Fig. 1(b), the superimposed spectra for $FPI_0 + FPI_1$ and $FPI_0 + FPI_2$ are obtained and are plotted in Figs. 2(c) and 2(d), respectively. The envelope signals that would be used for sensing applications are also indicated in the superimposed spectra. The FSR of the envelope signal in Figs. 2(c) and 2(d) is found to be ~1.04 GHz and ~0.73 GHz, respectively, which are close to the theoretical values (i.e., ~1.10 GHz and ~0.69 GHz) predicted by Eq. (4).

Next, an experiment was conducted to test the sensitivity-enhanced distributed sensing capability of the system shown in Fig. 2(a). Stress was applied to sensing FPI_1 and FPI_2 to stretch the two optical fiber sections. The applied stress elongated both fiber sections by 1200 μm in steps of 200 μm, whereas the fiber sections for reference FPI_0 and sensing FPI_3 were not disturbed. Figure 3(a) shows the reconstructed interferograms of FPI_1 and the envelope signals of superimposed spectra of $FPI_0 + FPI_1$ at ~3 GHz for different settings of length change. As can be seen, as the fiber length was increased, the dip frequency in the interferogram shifted to the low-frequency region. Interestingly, the dip frequency in the envelope signal shifted to the high-frequency region. This is because the OPD of FPI_1 (the sensing interferometer) was smaller than that of FPI_0 (the reference interferometer) resulting in a negative sensitivity amplification factor, as predicted by Eq. (5). The shift in dip frequencies as a function of length changes for both cases are plotted in Fig. 3(b). The sensitivity amplification factor was determined to be ~22 with a negative sign, which matched well with Eq. (5). Figure 3(c) shows the responses of FPI_2, including the reconstructed interferograms and superimposed spectra (i.e., $FPI_0 + FPI_2$) centered at ~2.2 GHz for different settings of length change. Since the OPD of FPI_2 is larger than that of FPI_0, the dip frequencies in both cases shifted to the low-frequency region. Figure 3(d) presents the shift in dip frequencies with respect to length change. The sensitivity amplification factor was found to be ~16, which again agreed with Eq. (5). Note that the interferograms of FPI_3 and FPI_0 and their superimposed spectrum did not show a significant shift in the experiment because these two fiber sections were not disturbed. This experiment demonstrates that by combining the OCMI system with the Vernier-effect-based technique, sensitivity-enhanced distributed sensing based on cascaded in-fiber reflectors (i.e., an FPI array) can be realized. The sensitivity amplification factor for each of the sensing FPIs depends on the OPD difference between the sensing FPI and the reference FPI.

For an ideal system, the OPD of the sensing FPIs should be identical or close so that large amplification factors for all the sensing FPIs can be obtained for a given reference FPI.

An additional experiment was performed to demonstrate that the sensitivity amplification factor for the sensing FPIs can be adjusted by changing the length of the reference FPI (i.e., FPI_0). The results are given in Fig. S1 in Supplement 1. Note that although only three FPIs were employed in the proof-of-concept demonstration limited by the lab facility, the capability of the OCMI technique is far beyond this limitation. The measured spatial domain signal of a modified system with eight cascaded FPIs in the sensing arm is presented in Fig. S2. By using the fs-laser direct writing technique to inscribe weak reflectors in an optical fiber core (with a typical reflectivity of approximately −45 dB) [17], thousands of reflectors can be cascaded along a single optical fiber, making long-distance and high-sensitivity distributed sensing possible with the assistance of the proposed technique. A theoretical analysis regarding the maximum multiplexing amount of FPIs is given in Supplement 1.

It is worth mentioning that the OCMI system operates at an incoherent setting so that the system is insensitive to the types of waveguides (single-mode fiber or multimode fiber), making it a good candidate for developing distributed multimode fiber-based sensors for harsh-environment applications [18,19]. However, the incoherent operation significantly limits the sensitivity and dynamic range of the OCMI system, at least one order of magnitude smaller than an OFDR system. It is quite challenging for an OCMI system to interrogate the Rayleigh backscattering signals along an optical fiber for distributed sensing. Therefore, weak reflectors are required for the enhancement of the signal-to-noise ratio, which increases the sensor cost compared with an OFDR system where an unmodified optical fiber is used as the sensing element. This work is dedicated to addressing the sensitivity aspect by proposing a technique that can increase the sensitivity of the OCMI system, making it comparable to the state-of-the-art OFDR systems. The OCMI system is advantageous in terms of system cost and the largest measurable length since large-bandwidth microwave components are readily available.

In conclusion, a sensitivity-enhanced distributed optical fiber sensor by combining the OCMI interrogation approach and the Vernier-effect-based sensitivity amplification technique has been proposed and experimentally demonstrated. The system included two arms, the sensing arm and the reference arm. A reference FPI was fabricated in the reference arm, whereas the sensing arm included cascaded in-fiber reflectors that formed a sensing FPI array. Using the OCMI interrogation approach, the interferogram of each of the sensing FPIs could be ambiguously reconstructed. By superimposing the reconstructed interferogram of a specific sensing FPI with the interferogram of the reference FPI, the Vernier effect was generated that could substantially improve the sensitivity of the sensing FPI by tracking the frequency shift of the envelope signal of the superimposed spectrum. In addition, the sensitivity amplification factor was shown to be dependent on the length difference between the sensing FPI and the reference FPI and could be easily adjusted by varying the length of the reference FPI. The work presented herein demonstrated the first implementation of the widely used Vernier-effect technique in a distributed optical fiber sensing system, and paves the way to develop high-sensitivity dark-zone-free distributed sensing systems that can find wide applications in structural health monitoring and other fields.

Funding. Research Initiation Project of Zhejiang Laboratory (113012-PI2201).

Disclosures. The authors declare no conflicts of interest.

Data availability. Data underlying the results presented in this paper are not publicly available at this time but may be obtained from the authors upon reasonable request.

Supplemental document. See Supplement 1 for supporting content.

REFERENCES

1. Y. Liu, X. Li, Y.-n. Zhang, and Y. Zhao, Measurement **167**, 108451 (2021).
2. T. Nan, B. Liu, Y. Wu, J. Wang, Y. Mao, L. Zhao, T. Sun, and J. Wang, Opt. Express **27**, 17239 (2019).
3. M. Quan, J. Tian, and Y. Yao, Opt. Lett. **40**, 4891 (2015).
4. T. Paixão, F. Araújo, and P. Antunes, Opt. Lett. **44**, 4833 (2019).
5. P. Zhang, M. Tang, F. Gao, B. Zhu, S. Fu, J. Ouyang, P. P. Shum, and D. Liu, Opt. Express **22**, 19581 (2014).
6. H. Liao, P. Lu, X. Fu, X. Jiang, W. Ni, D. Liu, and J. Zhang, Opt. Express **25**, 26898 (2017).
7. M. La Notte and V. M. Passaro, Sens. Actuators, B **176**, 994 (2013).
8. B. Wu, C. Zhao, B. Xu, and Y. Li, Sens. Actuators, B **255**, 3011 (2018).
9. X.-Z. Wang and Q. Wang, Sensors **18**, 4114 (2018).
10. M. La Notte, B. Troia, T. Muciaccia, C. E. Campanella, F. De Leonardis, and V. Passaro, Sensors **14**, 4831 (2014).
11. Z. Xu, X. Shu, and H. Fu, Opt. Express **25**, 21559 (2017).
12. Y. Zhang, B. Xu, D. Wang, H. Gong, Y. Li, and C.-L. Zhao, Opt. Fiber Technol. **43**, 175 (2018).
13. C. Zhu and J. Huang, Opt. Express **29**, 16820 (2021).
14. M. Islam, M. M. Ali, M.-H. Lai, K.-S. Lim, and H. Ahmad, Sensors **14**, 7451 (2014).
15. Z. Chen, L. Yuan, G. Hefferman, and T. Wei, Opt. Lett. **40**, 320 (2015).
16. Z. Chen, G. Hefferman, and T. Wei, IEEE J. Sel. Top. Quantum Electron. **23**, 246 (2017).
17. J. Huang, X. Lan, M. Luo, and H. Xiao, Opt. Express **22**, 18757 (2014).
18. J. Huang, X. Lan, Y. Song, Y. Li, L. Hua, and H. Xiao, IEEE Photonics Technol. Lett. **27**, 1398 (2015).
19. L. Hua, Y. Song, J. Huang, X. Lan, Y. Li, and H. Xiao, Appl. Opt. **54**, 7181 (2015).
20. L. Hua, Y. Song, B. Cheng, W. Zhu, Q. Zhang, and H. Xiao, Opt. Express **25**, 31362 (2017).
21. X. Zhu, L. Hua, J. Lei, J. Tang, L. Murdoch, and H. Xiao, Opt. Lett. **46**, 1173 (2021).
22. L. Hua, *Microwave Photonics for Distributed Sensing* (Clemson University, 2017).
23. C. Zhu and J. Huang, Opt. Lett. **46**, 2180 (2021).

131.151.26.204 on 2023-03-09 08:55:40